



GEO Québec  
2015

Challenges from North to South  
Des défis du Nord au Sud

# Improvement of the Piezo-electric Ring Actuator technique (P-RAT) using 3D numerical simulations

Ahmed Mhenni, Mahmoud N. Hussien & Mourad Karray  
Département de génie civil – Université de Sherbrooke, Sherbrooke, Québec, Canada

## ABSTRACT

Shear wave velocity of soil is commonly measured in the laboratory using piezoelectric elements such the bender elements (BE). These techniques, however, are associated with several difficulties including the mixed radiation of both primary and shear waves, near-field effects, boundary effects, and uncertain detection of first arrivals. A new technique, piezoelectric ring-actuator technique (P-RAT) has been developed in the geotechnical laboratory at the Université de Sherbrooke to minimize/eliminate the difficulties associated with other techniques, in particular, the penetrating of the used sensors into the tested specimens that may be inescapable in BE technique. This paper presents a brief description of the P-RAT technique as well as the results of 3D numerical simulations conducted using the computer code, COMSOL in order to study the interaction between the P-RAT components and the tested sample (soil or solid). This study demonstrate the effectiveness of the P-RAT technique and shows that the 3D simulations can be used in order to improve the reliability and/or the performance of the P-RAT to expand its applicability in the field of civil engineering.

## RÉSUMÉ

La vitesse des ondes de cisaillement est généralement mesurée en laboratoire en utilisant des éléments piézo électrique comme les Bender éléments (BE). Cependant, ces techniques présentent certains problèmes au niveau l'émission à la fois ondes primaires et de cisaillement, les effets de champ proche, les effets de bord, et l'incertitude au niveau de l'interprétation du signal. Une nouvelle technique, baptisé technique des anneaux piézoélectriques actionneurs (P-RAT) a été développé dans le laboratoire géotechnique de l'Université de Sherbrooke afin de minimiser / éliminer les difficultés associées aux autres techniques, en particulier, la pénétration des échantillons obligatoire pour la technique BE. Cet article présente une brève description de la technique P-RAT ainsi que les résultats des simulations numériques réalisées avec le code informatique, COMSOL afin d'étudier l'interaction entre les composantes du P-RAT et l'échantillon testé (sol ou solide). L'étude démontre l'efficacité du concept de la méthode P-RAT et montrent les simulations 3D peuvent être pour améliorer la fiabilité et / ou la performance de la méthode P-RAT afin d'étendre son applicabilité dans le domaine du génie civil.

## 1 INTRODUCTION

The importance of shear wave velocity ( $V_s$ ) has been widely recognized as a design parameter for soils subjected to dynamic loading. The past several decades have seen a significant increase in the use of  $V_s$  in geotechnical applications especially those involving earthquake ground response analysis, liquefaction potential, and soils characterization in terms of geotechnical and mechanical properties. Shear wave velocity can also be used to monitor setting and hardening of cement-based materials and also to characterize solid materials (rock, concrete, etc). Unlike most of the conventional geotechnical parameters such as N-SPT and  $q_c$ -CPT,  $V_s$  can be measured either in situ or in the laboratory on reconstituted or undisturbed soil specimens (Karray et al. 2011; Karray et al. 2015).

Shear wave velocity of soil is commonly measured in the laboratory using the resonant column (RC), the ultrasonic pulse (UP), and the piezoelectric bender element (BE) techniques. The results of these laboratory studies provide a wide database that can be implemented to address parameters which affect  $V_s$ . For this particular reason, the laboratory studies are more comprehensive and conclusive than the field measurements. However, the available laboratory techniques are associated with several difficulties including the mixed radiation of both

primary and shear waves, near-field effects, boundary effects, and uncertain detection of first arrivals. These difficulties, in fact, question the reliability of the experimental results obtained from the aforementioned techniques and limit their use to assess material stiffness.

A new technique, piezoelectric ring-actuator technique (P-RAT) has been developed in the geotechnical laboratory at the Université de Sherbrooke (e.g., Gamal El-Dean 2007; Ethier 2009; Karray and Ben Romdhan 2011; Ben Romdhan et al. 2014; Karray et al. 2015) in order to minimize/eliminate the difficulties associated with other techniques, in particular, the penetrating of the used sensors into the tested specimens that may be obligatory in the BE technique.

The most critical aspect that requires careful study and that can be done only by using numerical simulations is the effectiveness of the developed concept (P-RAT) to generate shear waves at the interface emitter-medium. This paper presents a brief description of the P-RAT technique as well as the results of 3D numerical simulations conducted with the computer code, COMSOL in order to study the interaction between the P-RAT components and the tested sample (soil or solid).

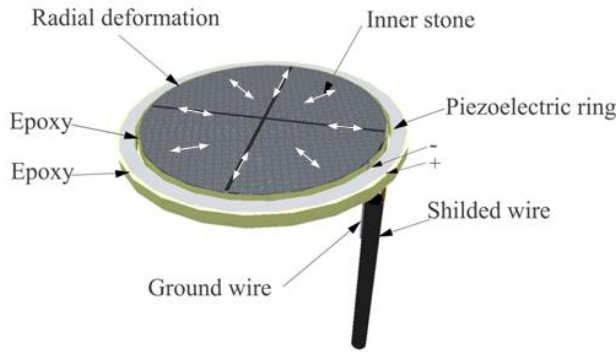


Fig.1 piezoelectric ring-actuator concept

## 2 THE PIEZOELECTRIC RINGS ACTUATORS TECHNIQUE (P-RAT)

The P-RAT was developed at Université de Sherbrooke (e.g., Gamal El Dean, 2007; Ethier, 2009 and Karray et al. 2015). The P-RAT can be incorporated into the conventional oedometer, triaxial or DSS apparatus. The P-RAT essentially consists of two parts: an emitter and a receiver (Fig. 1). These parts are fastened in the top and bottom heads of the oedometer, Triaxial or DSS cells. Each part (the emitter or the receiver) is a piezoelectric inert ring covered at its outer and inner faces by a thin conductive layer. Both faces are welded to shielded wires (Fig.1) that transfer voltage pulses with different durations and shapes. These voltage pulses cause the piezoelectric ring to vibrate in the radial direction (Fig. 1). A porous stone is fitted inside the ring using a special epoxy to allow the propagation of shear wave when the coupled ring-stone system is in contact with the soil specimen. The shearing of the sample is assured by the porous stone which is bordered by the ring. It imposes a radial movement to the four-pieces divided stone. This also gives P-RAT the ability to be used in different soil media under hard test conditions. The wave reaches the receiver ring where its velocity is measured after signal processing (Karray et al. 2015).

Soil deformations produced during P-RAT can be considered relatively low ( $\gamma < 10^{-3}\%$ ) and it can be assumed that the soil behaves linearly. As shown in Fig. 2, the whole test can be conceived as a system relating input and output signals (Karray et al. 2015).

## 3 THREE-DIMENSION (3D) NUMERICAL SIMULATION OF THE P-RAT

The 3D numerical simulation of the P-RAT was performed in this study with the computer code, COMSOL that presents an interactive interface with a rich library. The design of the sensors was directly imported, and the different components were identified: the Silicone, Epoxy, the piezoelectric ring, and the porous stone.

Comsol Multiphysics "Solid Mechanics" module was the main physics deployed for the model analysis. Models

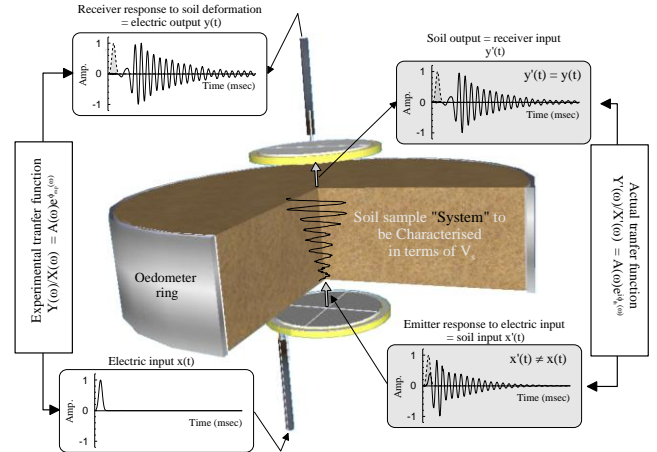


Fig 2. Schematic of experimental and actual transfer functions (Karray et al 2015).

based on wave propagation are generally assumed as a linear systems perspective; this approach is also useful here. The Solid Mechanics (solid) interface, found under the Structural Mechanics branch when adding a physics interface, is intended for general structural analysis of 3D, 2D, or axisymmetric bodies. The Solid Mechanics interface is based on solving Navier's equations, and results such as displacements, stresses, and strains are computed.

The Settings window for Material summarizes the predefined or user-defined material properties for a material. The Linear Elastic Material is the default material, which adds a linear elastic equation for the displacements and has a Settings window to define the elastic material properties.

$$\rho \frac{\partial^2 \mathbf{u}}{\partial t^2} = \nabla \cdot \mathbf{s} + \mathbf{F}_v \quad [1]$$

The total engineering strain tensor is written in terms of the displacement gradient:

$$\boldsymbol{\varepsilon} = \frac{1}{2} (\nabla \cdot \mathbf{u} + \nabla \cdot \mathbf{u}^T) \quad [2]$$

Hooke's law relates the stress tensor to the strain tensor and temperature:

$$\mathbf{s} = \mathbf{s}_0 + \mathbf{C} : (\boldsymbol{\varepsilon} - \boldsymbol{\varepsilon}_0 - \boldsymbol{\varepsilon}_{th}) \quad [3]$$

Where:

$\mathbf{C}$  is the 4<sup>th</sup> order elasticity tensor, ":" stands for the double-dot tensor product (or double contraction),  $\mathbf{s}_0$  and  $\boldsymbol{\varepsilon}_0$  are initial stresses and strains,  $\boldsymbol{\varepsilon}_{th} = \alpha(T - T_{ref})$  is the thermal strain, and  $\alpha$  is the coefficient of thermal expansion.

The system damping is represented using the Rayleigh Damping. In this damping model, the damping parameter  $\xi$  is expressed in terms of the mass  $m$  and the stiffness  $k$  as

$$\xi = \alpha_{dM} m + \beta_{dK} k \quad [4]$$

The piezoelectric effect is an interaction between the mechanical and electrical physics, where a stress applied on a piezoelectric material generates a voltage (direct effect) or a voltage applied on it generates the deformation of the material (inverse effect). In COMSOL Multiphysics, the Piezoelectric Devices multiphysics interface is constituted of one Solid Mechanics and one Electrostatics interface, which are coupled together by a Piezoelectric Effect multiphysics feature. Hence a piezoelectric problem contains solid and electrostatic domains, with at least one domain shared by the two physics interfaces and with the piezoelectric coupling defined on it. The piezoelectric can be defined by the following properties:

Mechanical Properties:

- Density,  $\rho$  (kg/m<sup>3</sup>)
- Elasticity matrix  $cE$  (Pa) in Stress-charge form.
- Compliance Matrix  $sE$  (1/Pa) in Strain charge form.

Electrostatic Properties:

- Relative Permittivity  $\epsilon S$  (1) in Stress-charge form.
- Relative Permittivity  $\epsilon T$  (1) in Strain-charge form.

Coupling properties:

- Coupling matrix  $eES$  (C/m<sup>2</sup>) in Stress-Charge form.
- Coupling matrix  $dET$  (C/N) in Strain-charge form.

Damping and loss properties:

- Loss factor for elasticity matrix  $cE$ ,  $\xi cE$ , or loss factor for elasticity matrix  $sE$ ,  $\xi sE$ : required when Mechanical Damping is present. The latter is valid only in Strain-Charge form.
- Loss factor for electrical permittivity matrix  $\epsilon rS$ ,  $\xi \epsilon rS$ , or Loss factor for electrical permittivity matrix  $\epsilon rT$ ,  $\xi \epsilon rT$ : required when Dielectric Loss is present. The latter is valid only in Strain-Charge form.
- Loss factor for coupling matrix  $e$ ,  $\xi eES$ , or loss factor for coupling matrix  $d$ ,  $\xi dET$ : required when Coupling Loss is present. The latter is valid only in Strain-Charge form.
- Electrical conductivity  $\sigma$  (S/m): required when Conduction Loss is present.

For the piezoelectric ring, the piezoelectric material was selected from the program library as the Lead Zirconate Titanate (PZT-5A).

The Piezoelectric Effect multiphysics coupling node passes the appropriate relative permittivity from the Piezoelectric Material node in the Solid Mechanics

interface (where it is specified together with the other material properties of the piezoelectric) to the Charge Conservation, Piezoelectric node in the Electrostatics interface. The Charge Conservation, Piezoelectric node implements the domain level electrostatics equations, and

requires no user settings when it is coupled with the multiphysics node.



Fig. 3. Actual and simulated piezoelectric sensor.

The coupled Constitutive equations for the Piezoelectricity in Stress-Charge Form :

$$T = c_E \cdot S + e^T \cdot E \quad [5]$$

$$D = e \cdot S + \epsilon_s \cdot E$$

Where :

$[T]_{6 \times 1}$ : Stress components (N.m<sup>-2</sup>)

$[S]_{6 \times 1}$ : Strain components (m.m<sup>-1</sup>)

$[E]_{3 \times 1}$ : Electric Field components (N.C<sup>-1</sup>)

$[D]_{3 \times 1}$ : Electric Charge Density Displacement Components (C.m<sup>-2</sup>)

$[cE]_{6 \times 1}$ : Stiffness coefficients measured under a constant or a zero electric field (N.m<sup>-2</sup>)

$[e]_{3 \times 6}$ : Piezoelectric coupling coefficients for Stress-Charge Form (C.m<sup>-2</sup>)

$[\epsilon_s]_{3 \times 3}$ : Electric Permittivity (F.m<sup>-1</sup>)

The 3D numerical model developed in this study gathers/simulates the different components involved in the manoeuvre of the piezoelectric sensor presented in Fig. 3:

- A layer of silicone, whose role is to seal the sensor and fix it on the top or the head of the apparatus.
- The layer of epoxy to protect from water and fix the piezoelectric ring to the porous stone,
- The piezoelectric ring element radially polarized actuator that used to convert the electrical pulses into lateral vibration and vice versa.
- The porous stone that was quartered to minimize the effect of compression and has an indented surface for better transmission of vibrations between the test sample and the sensor.

For the first phase, all the components were modeled with linear elastic model. The elastic properties used for the different components of the sensors are listed in Table 1. Being glued together, all the interfaces within the various components was related to one another, preventing slippage. The mesh is automatically

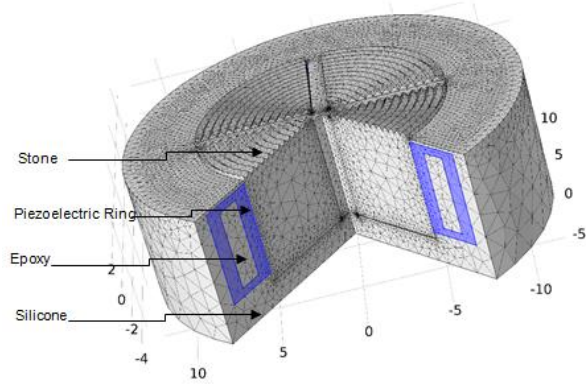


Fig. 4. General meshing of different components of the piezoelectric sensor

generated with “Comsol” using the “Fine” option. The general meshing of the different components is shown in Fig. 4. For the boundary conditions, the side surface and the bottom of the silicone layer were totally set for modal analysis.

Table.1: Mechanicals properties of different components

	Density (kg/m <sup>3</sup> )	Young's modulus (Pa)	Poisson's ratio
Epoxy	1300	5E9	0.30
Silicone	900	7E8	0.40
Stone	2700	12E12	0.25

#### 4 RESULTS AND DISCUSSIONS

As a first step of the current numerical investigation, a model analysis was performed. The solver was an Eigen-frequency type that provides the main resonant frequencies and the subsequent shapes, as shown in Fig. 5. Modal analysis results presented in Fig. 5 show that the fundamental mode, the predominant mode, has an exclusively radial nature, which proves the tendency of the ring to expand and contract radially and cause a subsequent lateral deformation on the surface of the porous stone that is responsible to generate shear waves in the tested sample. This result illustrates the exactness of the concept and the effectiveness of the P-RAT design to generate predominantly shear waves.

It is worth to mention here that the main objective of the development of the P-RAT is to produce a versatile system for measuring the shear wave velocity in a wide range of samples including cohesive and cohesionless soils. One of the key parameters to achieve that is to vary the resonance frequency of the sensor. Simulations with different values of stiffness of the silicone and epoxy layers shown in Fig. 5 have illustrated the direct influence of these two materials on the resonance frequency. The results of the P-RAT can be improved by experimenting different types of silicone and epoxy and associating each product stiffness range to the type of sample to be tested.

To further assess the effectiveness of the P-RAT to generate shear waves, another model with the sensor and a PVC cape, whose role is to keep the sensor and apply pressure on the sample was performed (Fig. 6), to compare between the lateral and longitudinal acceleration at different points of the surface following the application of an electrical pulse to the piezoelectric ring. Figure 7 shows a comparison between longitudinal and lateral accelerations at a selected point. Figure 7 shows that the maximum lateral acceleration is 3 times higher than the longitudinal acceleration, and the corresponding peak occurs earlier. The variation of the rigidity parameters of the silicone layer and the epoxy has also an impact on the amplitude of both the lateral and longitudinal accelerations, but the ratio of the two accelerations is always equal to 3. The later results is not presented in this paper due to the limitation in space. These results confirm the effectiveness of the adopted concept to generate shear waves.

To develop a model that correctly predict the response of the sensors in different situations, the effect of applied confining pressure on the sensor response was the target of the second phase of this study. In fact, the sensor damping properties are closely related to the value of the applied confining pressure, as evidenced in Fig 8, Figure 8 illustrates the effect of the increase in the applied stress on the receiver response time history through some experimentally face-to-face measured signals.

To include the effect of the confining pressure and calibrate/validate the proposed 3D numerical model against experimental measurements, a two-steps analysis modal has been performed:

- The first step, (static) to apply a pressure and redefine the mesh and the stress state in the model.
- The second step, (dynamic) to apply an electrical pulse to the electrodes of the transmitter and simulate the signal appearing on the receiver electrode.

Figures 9 show the results of numerical and experimental face-to-face tests (emitter on receiver) using two input signals (Ond1 and Chap6). Tests are conducted under a force of 1890 N. The signal (Chap6) is used to cover the widest possible range of frequency including the resonance frequency of the sensors (Fig. 1a and Fig. 1b). The energy content of the emitted signal is presented in Figs. 2a and 2b. The signal (Ond1) is used to avoid the resonance frequency of the sensors (Fig. 1c and Fig. 1d). The energy content of the emitted signal is also presented in Figs. 2c and 2d. Figs. 9 show that the response of the receiver (output) in time domain depends on the transmitted signal. When the generated transmission frequencies are below the resonance frequency of the system, it is found that the response of the receiver is similar to the transmitted signal (Fig. 9c and 9d). It is interesting to see that the experimental and the simulated result are very similar. These results demonstrate the effectiveness of the P-RAT technique and also the linearity of the emitter-receiver system for frequency under approximately the half of the resonant frequency. At

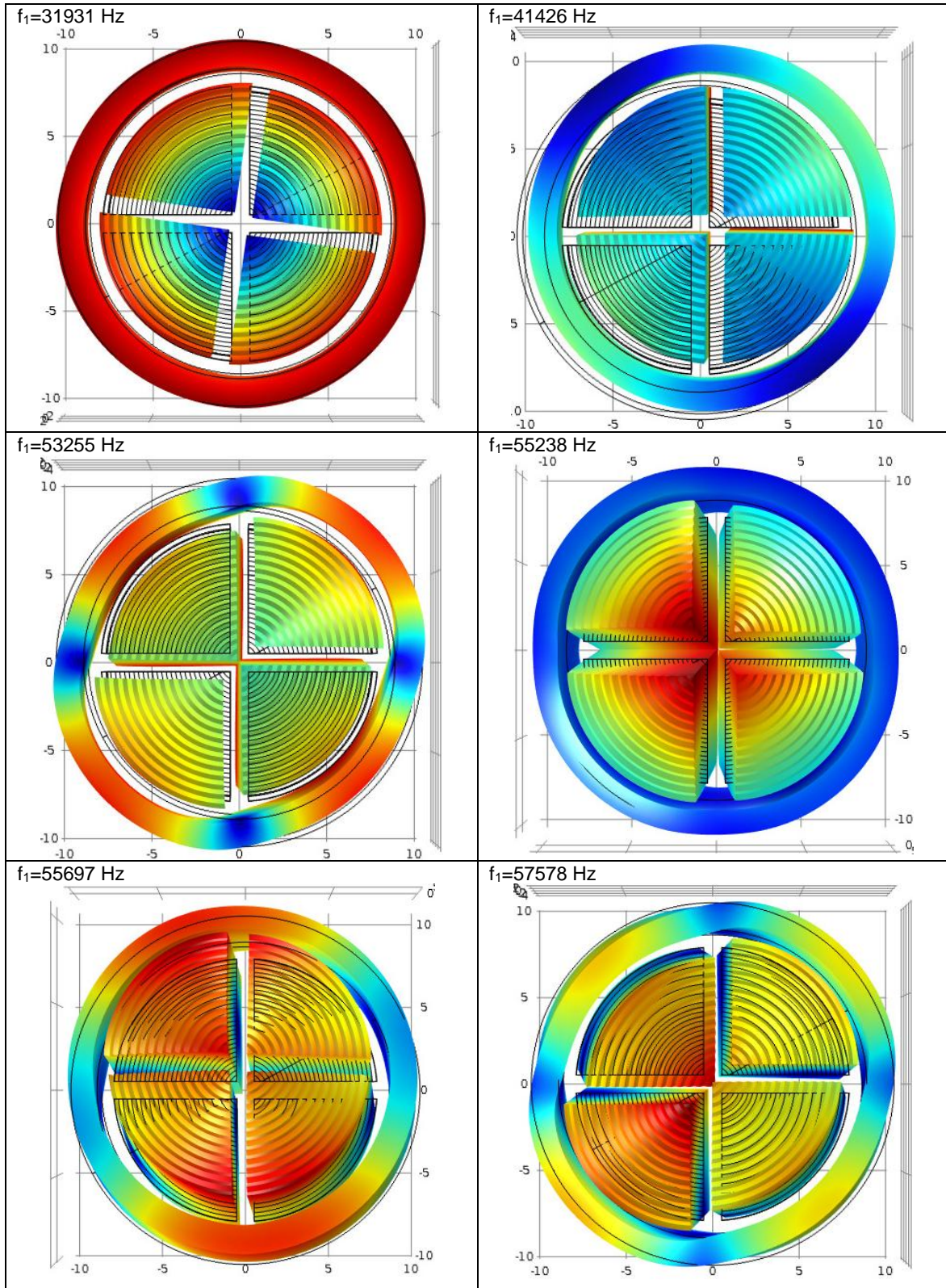


Fig.5. The main resonant frequencies and the subsequent shapes.

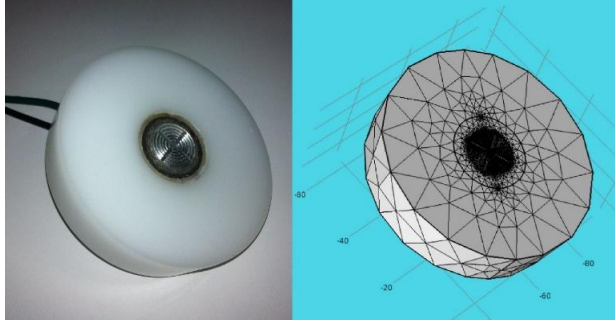


Fig. 6. Actual and simulated piezoelectric sensor with cap.

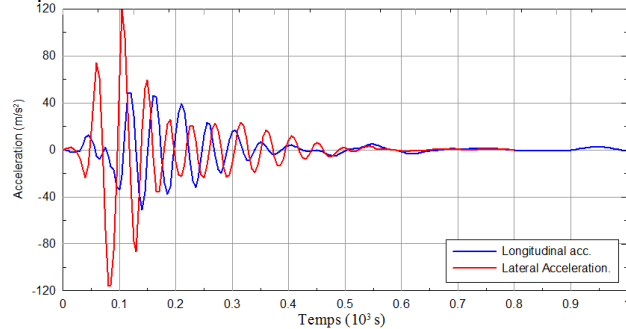


Fig. 7. Comparison between longitudinal and lateral accelerations.

this band of frequency there is no need to correct for the phase error produced by sensors.

Otherwise (Figs. 9a and 9b), the system produces undamped signals and clearly denotes resonance. In this case the experimental and numerical results are different due to the lack of determining the precise combination of material that allows having the same natural frequency. However, the behavior in the two cases is similar and confirm the difficulty of performing interpretation methods in time domain.

## 5 CONCLUSION

The results of a three-dimensional (3D) numerical simulation of the P-RAT, developed at the Université de Sherbrooke to minimize/eliminate the difficulties associated with other techniques of Vs measurements, are presented and discussed in this paper. The computer code, COMSOL is used for the computation in the current paper in order to study the interaction between the P-RAT components and the tested sample (soil or solid). Based on the presented results, the following conclusions are drawn:

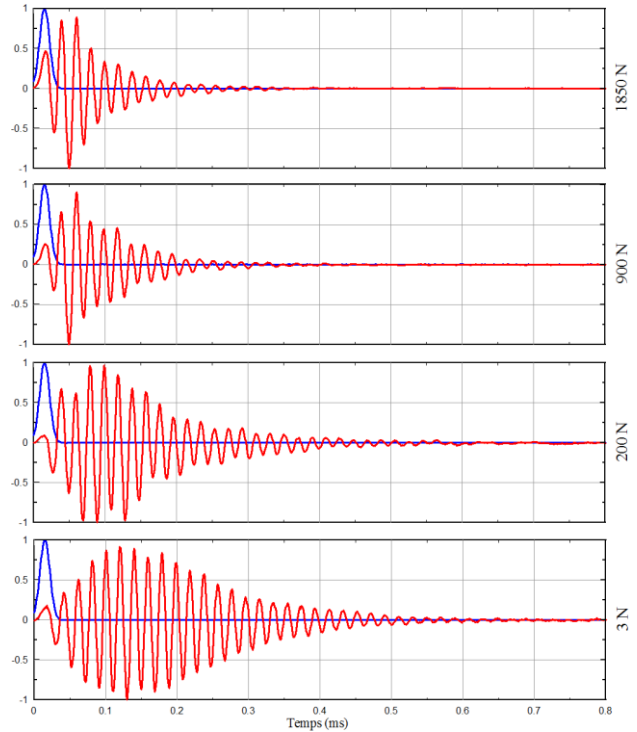


Fig. 8. Effect of the increase in the applied stress on the receiver response time history

1. The fundamental mode, the predominant mode, has an exclusively radial nature, which proves the tendency of the ring to expand and contract radially and cause a subsequent lateral deformation on the surface of the porous stone that is responsible to generate shear waves in the tested sample.
2. The variation of the rigidity parameters of the silicone layer and the epoxy has an impact on the amplitude of both the lateral and longitudinal accelerations, but the maximum lateral acceleration is always 3 times higher than the longitudinal acceleration. These results confirm the effectiveness of the adopted concept in designing the P-RAT to generate shear waves.
3. The experimental and numerical face-to-face tests prove that the P-RAT concept is appropriate to generate shear wave and also the linearity of the emitter-receiver system for frequency under approximately the half of the resonant frequency.

## ACKNOWLEDGEMENTS

The authors would like to thank the Natural Sciences and Engineering Research Council of Canada (NSERC) for their financial support throughout this research project.

## REFERENCES

- Ethier, Y.A. 2009. La mesure en laboratoire de la vitesse de propagation des ondes de cisaillement. Thèse de doctorat en génie civil, université de Sherbrooke.

Gamal El-Dean, D. 2007. Development of a new piezoelectric pulse testing device and soil characterization using shear waves. These de doctorat en genie civil, Université de Sherbrooke.

Karray, M., Ben Romdhan, M., Hussien, M. N., and Éthier Y., 2015. Measuring shear wave velocity of granular material using the piezoelectric ring-actuator technique (P-RAT). Canadian Geotechnical Journal 52: 1–16 dx.doi.org/10.1139/cgj-2014-0306.

Introduction to COMSOL Multiphysics 5.0, 2014, COMSOL Inc., MA, USA. Available: <http://www.comsol.com>.

COMSOL Multiphysics Reference Manual, Version 4.4, 2013, COMSOL Inc., MA, USA. Available: <http://www.comsol.com>.

Karray, M., Lefebvre, G., Ethier, Y., and Bigras, A. 2011. Influence of particle size on the correlation between shear wave velocity and cone tip resistance. Canadian Geotechnical Journal, 48(4): 599–615. doi:10.1139/t10-09.

Brissaud, M. 2007. Matériaux piézoélectriques : caractérisation, modélisation et vibration. Lausanne : Presses polytechniques et universitaires romandes.

Homepage of COMSOL Multiphysics 5.0 software (2015). Available from: <http://www.comsol.com>.

COMSOL Multiphysics User's Guide, Version 4.3, 2012, COMSOL Inc., MA, USA. Available: <http://www.comsol.com>.

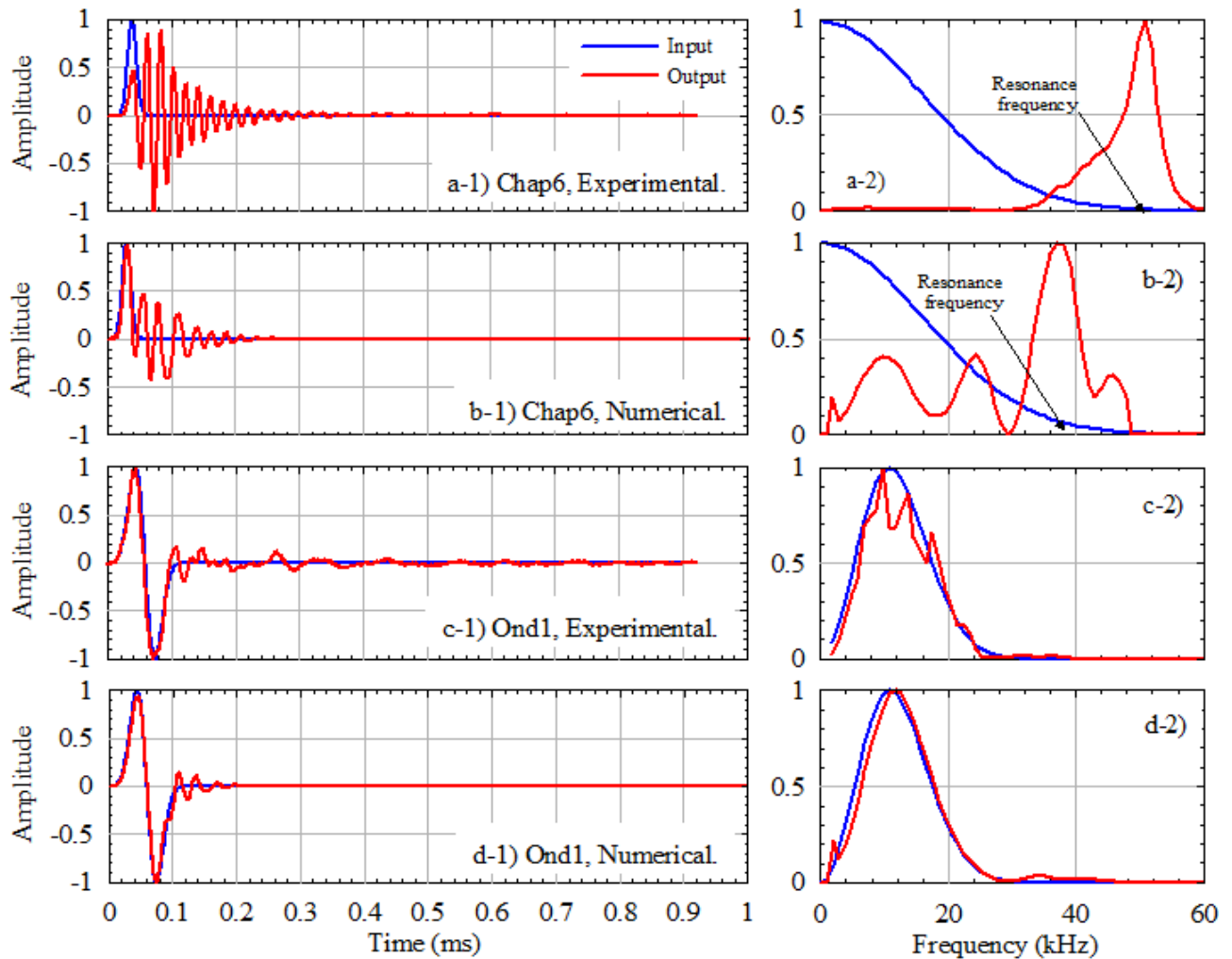


Fig. 9. Comparison between measured and computed signals.